Fatigue as a local phase decomposition: A switching-induced charge-injection model

X. J. Lou,* M. Zhang, S. A. T. Redfern, and J. F. Scott
Centre for Ferroics, Earth Sciences Department, University of Cambridge, Cambridge CB2 3EQ, United Kingdom
(Received 29 October 2006; published 6 June 2007)

Following our recent experimental work on electrical fatigue [Phys. Rev. Lett. **97**, 177601 (2006)], a theory of a charge-injection fatigue model is developed, emphasizing the extremely high depolarization electric field generated near the electrodes by bound charges at the tip of needlelike domains during switching. In particular, the relationship $P_r(N)/P_r(0) \sim \exp(-N/\lambda)$, where N is the number of the fatigue cycles and $\lambda \gg 1$, is derived, which explains the *statistical* origin of the *universality* of the logarithmic fatigue behavior observed for various ferroelectric substances in the literature. The consistency of this model with extensive body of the experimental data has been discussed and a systematic picture of fatigue is established. In particular, the "size effect"/fatigue coupling, the fatigue-free behavior of low P_r samples, and the exaggerated fatigue data of Colla *et al.* [Appl. Phys. Lett. **72**, 2478 (1998)] at very low frequencies (mHz) are all well predicted by our model.

DOI: 10.1103/PhysRevB.75.224104 PACS number(s): 77.80.Fm, 77.22.Ej, 77.80.Dj, 77.84.Dy

I. INTRODUCTION

Polarization fatigue, the decrease of switchable polarization during electrical cycling, has long been a serious, sometimes even mysterious, problem hindering the full commercialization of ferroelectric memories.[1,2] Although this phenomenon has been extensively investigated over the past decades, a single well-accepted model is still missing. Various explanations have been suggested over the past several decades, including 90° domains[1] and resultant strains, electromigration of existing vacancies to areas near the electrodes to form extended defects (or even to induce a percolative phase transition[3]) capable of pinning domains,[4,5] domain locking and/or pinning with electronic charge,[6] growth of a "dead and/or blocking layer,"[7–10] interface nucleation inhibition mechanisms induced by charge injection,[11,12] macro- and/or microcracking [for ceramic lead zirconate titanate (PZT)],[13] and so on. However, no model is fully consistent with the extensive body of experimental observations published in the literature. In particular, most of the models were developed in a rather qualitative way, with only a few exemptions.[4]

In our previous work, we show that fatigue (or rejuvenation) of the PZT film is caused by formation (or elimination after thermal reannealing) of degraded pyrochlorelike local regions induced by phase decomposition during bipolar electrical cycling.[14] [Note that our model is totally different from the scenario proposed by Lemanov and Yarmarkin, who believed that the preexisting pyrochlore phase (40–50 nm thick) at the near-electrode region of the virgin film during crystallization annealing and the resultant depolarization field are responsible for polarization fatigue.[15] Also note that electrode damage has also been found in bulk single-crystal $SrTiO_3$ after thermal treatment at elevated temperatures under reducing conditions.[16]] In the present paper, a different model of fatigue based on charge injection is developed.

II. A MODEL FOR FATIGUE

We are aware that the basic idea of charge injection as the primary culprit for fatigue has also been favored by other researchers, such as Melnick *et al.*,[17] Colla *et al.*,[11,12] and Mihara *et al.*[18]

Figure 1(a) (not to scale) shows the snapshot of the very early stage of the switching process after applying the first half of the ac field. The positive charges and negative charges are labeled by the plus and minus symbols, respectively. The bound charges are circled and the external charges (including the electrode screening charges) are uncircled. The left and right electrodes are shaded. The unshaded area represents a negative domain having spontaneous polarization pointing to the left, and the darker region represents a positive domain with polarization to the right. Figures 1(b) and 1(c) follow the same definitions. In order to simplify the illustration, the low-ε interface regions due to the imperfections and/or nonstoichiometry and/or strain and the space-charge regions due to oxygen vacancies and semiconductivity of ferroelectrics are not shown here, but will be discussed later.

After all these assumptions, Fig. 1(a) can be simplified into Fig. 1(b) by neglecting the compensated charges at the interfaces. It can be seen that the bound charges are totally unscreened, and therefore, a huge depolarization field at the electrode is expected under appropriate conditions, which will be discussed later. We note that Figs. 1(a) and 1(b) display a rather nonequilibrium transient state. The nucleation time is estimated to be 1 ns.[1] The forward growth time for a needlelike domain to propagate from one electrode to the other is estimated as[1]

$$t_{pg} = \frac{d}{v}, \tag{1}$$

where t_{pg} is the propagating time, d the film thickness, and v the speed of sound. By taking $d=400$ nm and $v=1000$ m/s, we have $t_{pg}=0.4$ ns, comparable with the fastest time ($\sim$220 ps) measured so far.[19] (Note that in the latter case, nucleation may occur not only at the interface but also in the middle of the film.) After that, the time for sideways growth will take a further few nanoseconds to microseconds, depending on the applied field, ramping rate, and limited by the RC time constant of the external circuits. Note that we ex-

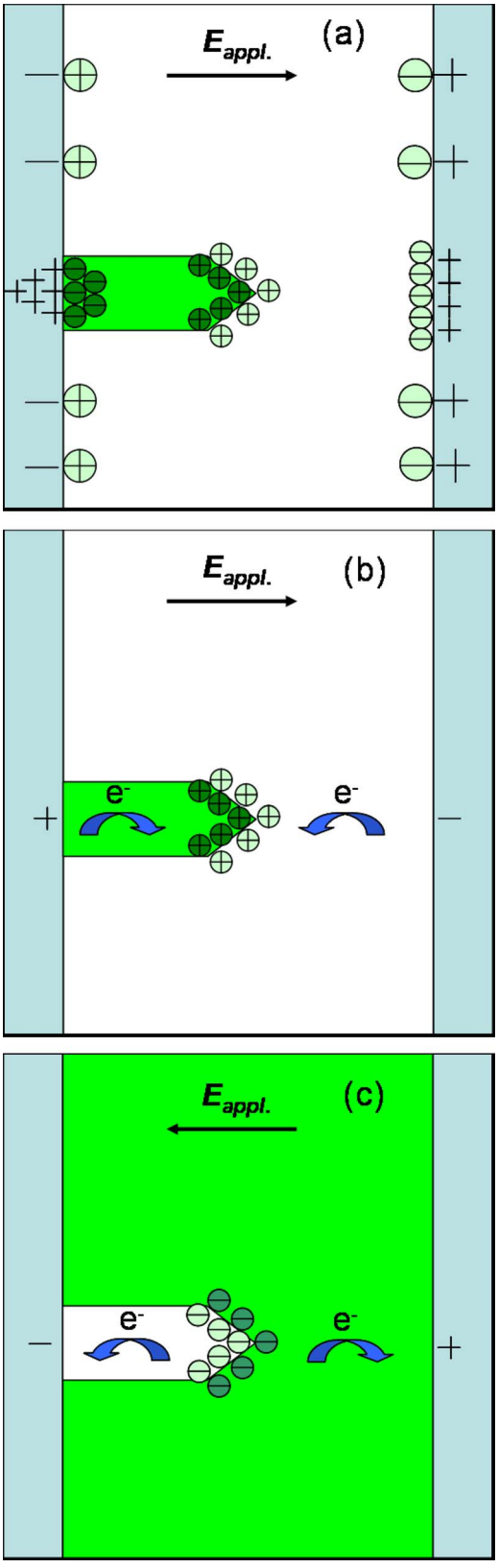

FIG. 1. (Color online) The snapshot of the nonequilibrium transient state at the very early switching stage (a); the simplified (a) is shown in (b) after ignoring all the compensated charges at the interfaces. (c) shows the equivalence of (b) by applying the second half ac field. Note that these figures are not to scale.

pand and generalize the meaning of t_{pg} to be the time covering both the propagating time defined above and the time that the nucleus is in its embryonic state t_{em} after its formation. t_{em} may have nothing to do with standard high-frequency fatigue measurements, where it is almost constant, and may also be of the order of nanoseconds, the same as the nucleation time, but will be crucial when we discuss the extremely low frequency studies later on.

There is no report on the geometry of the nucleus and the subsequent needlelike domains for thin-film ferroelectrics. It is reasonable to assume that the nuclei are on the order of nanometers in diameter and grow into high-aspect-ratio needles subsequently for standard thin-film ferroelectrics, similar to the bulk ferroic system.[20] Therefore, the head-to-head positive charges on the tip of the needle domain [Fig. 1(b)] can be reasonably treated as a point charge of $2P_rS_n$, where P_r is the remanent polarization and S_n the cross-section area of the needlelike domain. The depolarization field of these transient bound charges at the electrode can be readily calculated as follows:

$$E_{bc} = \frac{2P_rS_n}{4\pi\varepsilon_i\varepsilon_0 d_e^2}, \tag{2}$$

where d_e is the distance between the bound charges and the electrode, or the length of the needle domain. ε_i is the dielectric constant at the interface. In order to make numerical estimates, we will insert typical values for ferroelectric oxides, such as ferroelectric barium strontium titanate or rather mediocre PZT. Taking $P_r=20\ \mu\text{C/cm}^2$, $S_n=25\pi\ \text{nm}^2$, and $\varepsilon_i=40$ (we simply assume that it is 1 order of magnitude less than the bulk value due to the so-called dead and/or blocking layer,[21,22] and we will justify this assumption and emphasize the importance of ε_i later on), we have

$$E_{bc} \sim 70.58\left(\frac{nm^2}{d_e^2}\right)\frac{\text{MV}}{\text{cm}}, \tag{3}$$

where d_e^2 is in units of nm^2. Note that the real value of E_{bc} might be larger due to the "image charge" effect. Additionally, the static dielectric constant should be used in Eq. (2) rather than its optical equivalent, because $t_{pg}(\sim 10^{-10}\ \text{s})$ is still much larger than the period of an optical phonon $(\sim 10^{-13}-10^{-12}\ \text{s})$.

If the head-to-head charges propagate to the center of the film, we have $d_e=200$ nm. Putting this value into Eq. (3), we have $E_{bc}\sim 2$ kV/cm, a negligible value. However, when the nucleus is at its *embryonic stage* (i.e., when it is just about to propagate from the left electrode) or when it closely approaches the right electrode (in the latter case, d_e is equal to d, the film thickness, minus the length of the needle domain), d_e is of the order of a few nanometers, comparable to its lateral size. In this case, Eq. (2) derived from ideal point-charge assumption is no longer precisely true, but the relationship $E_{bc}\sim P_rS_n/\varepsilon_i\varepsilon_0 d_e^2$ still holds. Numerically, we can calculate E_{bc} generated for any shape of the nucleus. Particularly, supposing the nucleus has hemisphere geometry, a standard surface integral gives E_{bc} precisely to be

$$E_{bc} = \frac{P_r}{3\varepsilon_i \varepsilon_0}. \quad (4)$$

Again putting $P_r = 20\ \mu C/cm^2$ and $\varepsilon_i = 40$ into Eq. (4), we have $E_{bc} = 1.88$ MV/cm, an extremely high field, which is even higher than the *average* (not the real) breakdown field of the PZT films;[23] the nuclei have to withstand this high field twice for each electrical fatigue cycle. Taking the external charges into consideration [Fig. 1(b)], E_{bc} will be slightly lower when the bound charges are near the left (anode) electrode and slightly higher when they are near the right (cathode) electrode.

Note that unlike Eq. (2), E_{bc} does not depend on any geometric variables, such as hemisphere radius r in Eq. (4). That is reasonable, because S_n ($\sim \pi r^2$, r the radius of the cross section of the needle domain) follows the same scaling behavior as d_e^2 when the needle becomes shorter and shorter; hence they cancel each other in Eq. (2). Therefore our argument above is not restricted by the real geometry of the nucleus, at least to first order. It should be noted that $E_{bc} = 1.88$ MV/cm is by no means the upper limit of its achievable value. The spatial fluctuation of P_r (which can go up to $\sim 70\ \mu C/cm^2$ in ceramic films) the image charge effect and more rounded nucleus tips may push E_{bc} further into ~ 10 MV/cm region, close to the interface breakdown field which may be (although still controversial) 1 order of magnitude higher than the measured value if the voltage drop through the film is not uniform (linear). This is why films very often breakdown quickly before they are totally fatigued during standard fatigue measurements.

Note that the external field is on the order of ~ 100 kV/cm for thin films. The depletion field at the electrode can be estimated via[24]

$$E_{bi} = \frac{qN_dW}{\varepsilon\varepsilon_0}, \quad (5)$$

where q is the electron charge, N_d the space-charge density, W the depletion width, and ε and ε_0 the static dielectric constant of the ferroelectric and permittivity of free space, respectively. Setting $N_d = 10^{19}\ cm^{-3}$, $W = 20$ nm (assume the film is only partially depleted), and $\varepsilon = 400$, we have $E_{bi} \sim 100$ kV/cm. The converse assumption of full depletion with $N_d = 10^{18}\ cm^{-3}$ and $W = d/2 = 200$ nm gives the same E_{bi}. The depolarization field is of the same order, depending on the interface screening ability. Therefore they are all 1 or even 2 orders of magnitude less than the field we calculated above and can be all safely neglected.

Therefore, the left (or right) electrode is experiencing an *extremely* high transient electrical field (1–10 MV/cm) when the needlelike domain leaves from the left electrode (or approaches the right one). The injected current from the electrode is most likely to be determined by Fowler-Nordheim tunneling via

$$J = C_{FN}E_{bc}^2 \exp\left(-\frac{4\sqrt{2m^*}(q\phi_B)^{3/2}}{3q\hbar E_{bc}}\right), \quad (6)$$

where C_{FN} is the Fowler-Nordheim coefficient, which depends on the barrier height ϕ_B and the electron effective mass m^* at the interface. Microscopically, the energetic electrons injected will interact with the defects and phonons at the interface so as to increase the local temperature within and near the needlelike domain. The temperature will increase at a rate depending on the heat capacity of the material, its conductivity, and temperature gradient until the forward growth is finished. However, we believe that the heat loss due to conductivity at this stage can be ignored since the time scale is about ~ 0.1 ns. The local temperature starts to decrease during the subsequent sideways growth, at which stage its conductivity and temperature gradient become dominant. The local temperature increases and decreases during each cycle, and thermal equilibrium will be built up between the bulk film and the environment after a certain number of cycles. If the transient local temperature increases beyond some critical value, local phase decomposition will take place *stochastically*, as we have observed in this work and will be modeled in detail. In addition, the energetic electrons could also interact readily with the bound charges of the ions, and the subsequent de-ionization will generate more defects and vacancies (e.g., $V_o^{\cdot\cdot}$),[18,25] which can make the perovskite structure less stable against increased local temperature due to electron-phonon interactions. The equivalent picture during the second half of the ac field is depicted in Fig. 1(c). This stage is believed to be less important than that shown in Fig. 1(b) because of the limitation of the number of the carriers inside the film.

The temperature increase, sometimes called "self-heating," during switching cycles has been studied in bulk ferroelectrics, but not much attention has been paid to this phenomenon in thin films. The loss of energy can be visualized macroscopically from the total area within the characteristic hysteresis loops. Lente and Eiras[26] measured the temperature increase during the fatigue of their PZT ceramics. In their study, an increase of sample temperature up to 90 and 160 °C was observed under different conditions. It should be noted that the sample temperatures measured by Lente and Eiras are averaged ones, not the local temperatures we discussed above, which are expected to be much higher. Nevertheless, their observations strongly support our model.

The exact local temperature during fatigue is unknown and very difficult to measure. Let us set this problem aside and review the work in the literature on high-T PZT decomposition instead. Chen and Chen reported a Pb-deficient pyrochlore-type phase of $PbTi_3O_7$ appearing at 800 ° C when PbO rapidly evaporates.[27] Castellano and Feinstein also observed that the perovskite structure collapsed into the pyrochlore phase due to loss of oxygen when the sample was heated to 800 ° C.[28] Additionally, phase decomposition in PZT has been reported at a temperature as low as 550 ° C.[29] It is noted that the phase decomposition is very sensitive to the concentration of oxygen vacancies, with the critical concentration estimated to be 15% by Castellano and Feinstein. Although the detailed phase diagram of the stability of the perovskite structure as a function of temperature and vacancies is unknown, a decrease of critical temperature as a function of the concentration of vacancies is reasonably expected.

Phase decomposition can induce fatigue in two ways: On one hand, the field applied on the film becomes significantly reduced after decomposition due to the low dielectric con-

stant of the degraded layer, i.e., a series capacitor structure forms (pyrochlore has $\varepsilon \sim 30$, 1 order of magnitude less than that of PZT); on the other hand, it can be seen that the most probable sites where the phase decomposition occurs are the domain nucleation sites [Fig 1(b)]. The decrease of the number of the available nucleation sites during electrical cycling also makes switching more difficult.

Having justified the physical scenario of this model, let us develop it quantitatively. Suppose originally there are totally M_0 nucleation sites on the left and right electrodes. The total number of the nucleation sites will reduce to M after N fatigue cycles. Let us suppose that the probability that decomposition will occur for a nucleation site after one cycle is $1/\lambda$ with $\lambda \gg 1$, which is assumed to be constant and independent of fatigue history (i.e., the cycling numbers N) at the moment, for simplicity. Therefore, the probability that a nucleus will survive from one cycle is $[1-(1/\lambda)]$. Defining that $g(N)$ is the probability that a nucleation site will survive after N cycles, we have

$$g(N) = \left(1 - \frac{1}{\lambda}\right)^N. \tag{7}$$

Therefore the total number of the nuclei which have survived from degradation after N cycles is

$$M(N) = M_0 g(N) = M_0 \left(1 - \frac{1}{\lambda}\right)^N. \tag{8}$$

Suppose that all these M_0 nuclei are randomly distributed over the electrodes' interfaces. Collapse of each nucleus, induced by phase decomposition, will stop the surrounding area or the associated grain from contributing or make them contribute little (recall the formed series capacitor structure with $\varepsilon \sim 30$ for pyrochlore) to the total remanent polarization. For simplicity, let us assume the remanent polarization $P_r(N)$ measured experimentally after N cycles is proportional to $M(N)$, the number of the survived nuclei, which yields

$$\frac{P_r(N)}{P_r(0)} = \frac{M}{M_0} = g(N) = \left(1 - \frac{1}{\lambda}\right)^N \tag{9}$$

Let us simplify Eq. (9) by recalling that $\lambda \gg 1$. Taking the natural logarithm on both sides of Eq. (9), we have

$$\ln g(N) = N \ln\left(1 - \frac{1}{\lambda}\right) = N\left[-\frac{1}{\lambda} - \frac{1}{2}\left(\frac{1}{\lambda^2}\right) + \cdots\right]. \tag{10}$$

Since λ is much larger than 1, all the higher-order terms can be neglected. So we get

$$\frac{P_r(N)}{P_r(0)} = g(N) = \exp\left(-\frac{N}{\lambda}\right). \tag{11}$$

Therefore, we arrive at an important conclusion from our model that $P_r(N) \sim \exp(-N/\lambda)$. The visualization of Eq. (11) is shown in Fig. 2 with $\lambda = 10^4$, 10^5, 10^6, and 10^7, respectively, which are believed to be the representing values for ferroelectrics (recall that $1/\lambda$ is the decomposition probability per cycle). Figure 2 explains the statistical origin of the *universality* of the logarithmic dependence of $P_r(N)$ on N observed for all kinds of ferroelectrics during fatigue measurements.

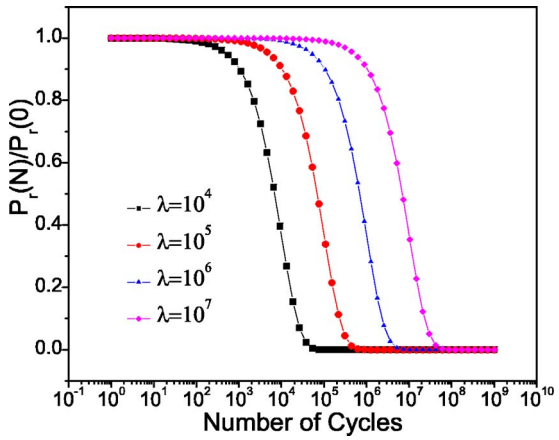

FIG. 2. (Color online) Plots of $P_r(N)/P_r(0)$ as function of cycle number N, according to Eq. (11), where $\lambda = 10^4$, 10^5, 10^6, and 10^7, respectively.

So far, the meaning of $1/\lambda$ is a little obscure and very statistical. In particular, $1/\lambda$ has no relationship with any micro and/or macroscopic measurable physical quantities. Let us go further and assume that the degradation probability $1/\lambda$ is a monotonically *increasing* function h of the local input power density $E_{bc}J$ at the nucleation site. This assumption can be justified as follows: the more energy the injected electrons carry, the more energy they will lose due to collision with the lattice at the tip of the nucleus, and therefore the more chance local decomposition takes place.

Considering Eq. (6), we have

$$\frac{1}{\lambda} = h(E_{bc}J) = h\left[C_{FN}E_{bc}^3 \exp\left(-\frac{4\sqrt{2m^*}(q\phi_B)^{3/2}}{3q\hbar E_{bc}}\right)\right] \tag{12}$$

and therefore Eq. (11) becomes

$$\frac{P_r(N)}{P_r(0)} = \exp\left\{-Nh\left[C_{FN}E_{bc}^3 \exp\left(-\frac{4\sqrt{2m^*}(q\phi_B)^{3/2}}{3q\hbar E_{bc}}\right)\right]\right\}. \tag{13}$$

For the simplest case where h is a linear function, we have

$$\frac{1}{\lambda} = AC_{FN}E_{bc}^3 \exp\left(-\frac{4\sqrt{2m^*}(q\phi_B)^{3/2}}{3q\hbar E_{bc}}\right) + B. \tag{14}$$

When $E_{bc}J$ goes to zero, physically $1/\lambda$ should also go to zero; therefore B must be zero. A is the decomposition probability per unit power density per cycle and is assumed to be a positive constant and is independent of E_{bc} and N for simplicity.

The function h relates the decomposition probability $1/\lambda$ to the local injected power density $E_{bc}J$. It depends on many unknown microscopic parameters and can be very complex. h could be a linear, power law, or exponential function. Its detailed form may be possibly derived by fitting the carefully measured experimental data.

We argue that the linear approximation is a rather conservative assumption. Intuitively, if $E_{bc}J$ is very small, $1/\lambda$ should be zero and therefore A must be zero; while, when $E_{bc}J$ becomes very large with E_{bc} close to the breakdown field E_B, $1/\lambda$ should be much larger than zero and close to 1; therefore A must be a finite number. However, we will show later on that for many purposes of application the linear approximation is a rather good tool, especially when we regard A as an experimental fitting parameter and allow it to increase with $E_{bc}J$.

Inserting Eq. (14) into Eq. (11) and noting that $B=0$, we have

$$\frac{P_r(N)}{P_r(0)} = \exp\left[-NAC_{FN}E_{bc}^3 \exp\left(-\frac{4\sqrt{2m^*}(q\phi_B)^{3/2}}{3q\hbar E_{bc}} \right) \right] \tag{15}$$

and inserting Eq. (4) into Eqs. (13) and (15), we have

$$\frac{P_r(N)}{P_r(0)} = \exp\left\{ -Nh\left[\frac{C_{FN}P_r^3}{27\varepsilon_i^3\varepsilon_0^3} \times \exp\left(-\frac{4\sqrt{2m^*}(q\phi_B)^{3/2}\varepsilon_i\varepsilon_0}{q\hbar P_r} \right) \right] \right\} \tag{16}$$

for the general case, and

$$\frac{P_r(N)}{P_r(0)} = \exp\left[-AN\frac{C_{FN}P_r^3}{27\varepsilon_i^3\varepsilon_0^3} \exp\left(-\frac{4\sqrt{2m^*}(q\phi_B)^{3/2}\varepsilon_i\varepsilon_0}{q\hbar P_r} \right) \right] \tag{17}$$

for the linear case. Note that $P_r \equiv P_r(0)$. It does not change during the fatigue process. It should be noted that P_r is very different from $P_r(N)$, which is the average value experimentally measured after N cycles.

Let us make a few remarks here about this model.

(a) Mathematically, the left-hand sides of Eqs. (16) and (17) go to zero when N approaches infinity. This is rather an ideal case. Experimentally, it has been generally observed that $P_r(N)$ starts to saturate at $N \sim 10^8$ cycles (this value varies depending on the type of the samples). Regarding our model, the collapse of all the nuclei, induced by local decomposition, does not make $P_r(N)$ totally vanish, but permits the existence of a small fraction of the remanent polarization [recall that although pyrochlore has $\varepsilon \sim 30$, a small fraction of E_{appl} on the bulk film still induces a measurable amount of $P_r(N)$]. Another reason for nonvanishing remanent polarization is due to the polycrystalline nature of the thin films. Grains having spontaneous polarization at small angles from the plane of the film contribute little to the total remanent polarization, but also show less fatigue (the orientation dependence of fatigue properties will be discussed later on). Therefore, instead of Eq. (17), for the linear case we have

$$\frac{P_r(N)}{P_r(0)} = D\exp\left[-AN\frac{C_{FN}P_r^3}{27\varepsilon_i^3\varepsilon_0^3} \exp\left(-\frac{4\sqrt{2m^*}(q\phi_B)^{3/2}\varepsilon_i\varepsilon_0}{q\hbar P_r} \right) \right] + F, \tag{18}$$

where $P_r(0)D$ and $P_r(0)F$ are the "fatigued" and "nonfatigued" remanent polarization, respectively, when N goes to infinity with $D+F=1$. F is normally much less than D.

Taking $m^*=0.5m_e$, $\phi_B \sim 1.5$ eV, and replacing AC_{FN} by a new coefficient A for convenience, we then have

$$\frac{P_r(N)}{P_r(0)} = D\exp\left[-5.34\times 10^{25}A\frac{NP_r^3}{\varepsilon_i^3} \exp\left(-23.57\frac{\varepsilon_i}{P_r} \right) \right] + F. \tag{19}$$

Note that P_r is in unit of $\mu C/cm^2$.

(b) In Eqs. (14) and (15) under the linear approximation, we assume that A is a constant and independent of N. This is equivalent to saying that $1/\lambda$, the decomposition probability, is independent of N. In other words, the degradation is equally probable for all the nuclei after each fatigue cycle. Again, this is an ideal assumption. In reality, some nucleation sites may be less resistive to phase degradation than others. Allowing the N dependence of $A(N)$ or $1/\lambda(N)$ may give a better data fitting for some ferroelectric samples by changing the slope at the "logarithmic stage," where P_r decreases markedly. In this case, Eq. (11) should be written as

$$\frac{P_r(N)}{P_r(0)} = g(N) = \exp\left[-\frac{N}{\lambda(N)} \right]. \tag{20}$$

(c) From Eq. (19), it can be seen that $P_r(N)$ only depends on N, P_r, ε_i, and possibly $A(N)$. None of the others is an adjustable parameter. This makes the problem much simpler, because all the other variables can be simply put into this equation via P_r (T, E_{appl}, f, crystallographic orientation, etc.), where T is temperature, E_{appl} the applied field, and f the frequency. Crystallographic orientation could be a variable if the sample is a single crystal.[30]

ε_i, the interface dielectric constant, may also depend on $E_{bc}(P_r(T,E_{appl},f),\varepsilon_i)$ via Eq. (4) as the bulk value ε does (recall the butterfly-shaped ε-E_{appl} curve and that the dielectric relaxation time is $\sim 10^{-12}$ s, much less than t_{pg}). But this issue is very subtle, since even the real value of ε_i and the related dead-layer thickness in the size effect topic haven not been clearly identified yet, not to mention its value under high E_{bc}. If there were a field dependence of ε_i, the real $\varepsilon_i(E_{bc})$ can be calculated self-consistently, provided the circular relationship $\varepsilon_i \sim \varphi(E_{bc}(P_r,\varepsilon_i))$ is given.

In this work, we simply assume that ε_i is constant, ~ 40 for films with dead and/or blocking layer showing size effect (e.g., Pt/PZT/Pt structure) and ~ 400 for those without this layer (e.g., Pt/SBT/Pt or IrO_2/PZT/IrO_2). The justification of $\varepsilon_i \sim 40$ is as follows: Work from Larsen *et al.*[7] shows that $\varepsilon_i/d_i = 20-28$ nm^{-1}, comparable with the study from Lee and Hwang, which gives $\varepsilon_i/d_i = 10.42-20.83$ nm^{-1} depending on the annealing conditions.[31] Furthermore, Lee and Hwang argued that d_i is on the order of 1 nm, then they concluded that ε_i must be on the order of 10–20. Here, we take a relatively conservative assumption that $\varepsilon_i/d_i = 20$ nm^{-1}. Taking $d_i = 2$ nm, we have $\varepsilon_i = 40$, which is 1 order of magnitude less than the bulk value.

Before we step into the next section, let us mention the work by Duiker *et al.*[32] The model of Duiker *et al.* assumes

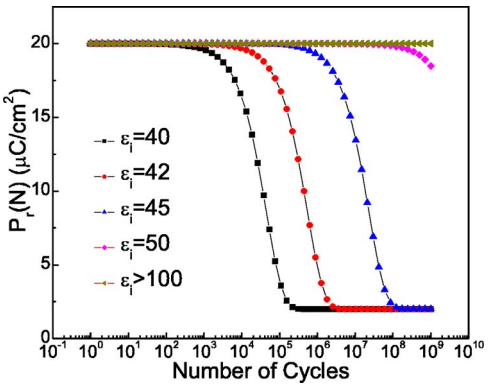

FIG. 3. (Color online) Plots of $P_r(N)$ as function of cycle number N, according to Eq. (19), where ε_i=40, 42, 45, 50, and >100, respectively. Here we take P_r=20 μC/cm^2, D=0.9, F=0.1, and $A=10^{-9}$.

that fatigue is induced by growing dendritic trees formed by permanently attached oxygen vacancies. During the fatigue process, the regions enclosed by the dendritic trees are screened and therefore contribute little to the total remanent polarization. Interestingly, by assuming a linear (or exponential) dependence between vacancy generation and applied field, a soft (or hard) failure is predicted by Monte Carlo simulations.

Recall that $E_{bc} \sim P_r/\varepsilon_i\varepsilon_0$ in our model and it does not depend on the size of the sample and the geometry of nuclei, at least to first order. Therefore our model is not restricted to thin-film ferroelectrics. It applies equally well to ceramic and single-crystal ferroelectrics.

III. FERROELECTRIC FATIGUE: INFLUENCE OF EXPERIMENTAL PARAMETERS

Here we will discuss some important implications of the current model and its consistency with the abundant experimental data in the literature.

A. Size effect and fatigue

Many researchers have noticed that fatigue phenomena are always accompanied by the appearance of thickness dependent electrical properties, i.e., the so-called size effect.[7,8,12,33] From Eq. (2) or (4), E_{bc} is proportional to P_r and reversibly proportional to ε_i, the dielectric constant of the interface layer. As we discussed above, 1 order of magnitude less of ε_i compared to its bulk equivalent ε, achieved by simply changing oxide/PZT/oxide to Pt/PZT/Pt structures, can readily shift E_{bc} to 1–10 MV/cm regions; therefore degradation and fatigue can easily occur. Although 1 order of magnitude increase of P_r may have the same effect, in principle, according to Eq. (4), in practice large increases in polarization are less often found. This explains why ε_i qualitatively determines whether a film will fatigue or not[7,8,12,33] and P_r only affects it quantitatively [see Fig. 12(a) in Ref. 30]. The ε_i dependence of $P_r(N)$ according to Eq. (19) has been plotted in Fig. 3 with ε_i=40,42,45,50,>100, respectively, where we take P_r=20 μC/cm^2, D=0.9, F=0.1, and $A=10^{-9}$ (in practice, A can be obtained by fitting the experimental data. It is important that A, the degradation probability per unit power density per cycle, should be a constant for a specific sample in an ideal case).

It can be seen from Fig. 3 that the lower the ε_i, the smaller the $P_r(N)$ will be if N and all the other variables in Eq. (19) are the same. Also shown is the extremely sensitive ε_i dependence of $P_r(N)$; ε_i increasing only from 40 to 50 corresponds to a fatigue resistivity dramatically increased to 5 orders of magnitude. It exactly explains why Pt/PZT/Pt fatigues and M_{oxide}/PZT/M_{oxide} (or Pt/SBT/Pt) does not and why fatigue is always coupled with size effect.

B. Dead layer and locality

Although a so-called growing dead-layer fatigue model is frequently employed to interpret fatigue data, such a layer has never been established by methods such as transmission electron microscopy. Our results[14] show that the degraded regions are probably around the nucleation sites, rather local, isolated, and not planar, although we are not sure what their exact size is currently (they should be about a few nanometers in thin films, although they can be much larger in bulk ferroelectrics). (Our results are compared with the work by Colla *et al.*[34] and Gruverman *et al.*[35]) The full percolation of the local degraded layers appears possible after many cycles from our preliminary data. But we believe that it occurs only in the "saturated stage" of fatigue and have nothing to do with the logarithmic stage where P_r decreases dramatically.

Polishing the surface of a fatigued PZT pellet and subsequent recovery of the polarization are consistent with our model.[36]

C. Fatigue and the virgin remanent polarization

Fatigue has been extensively studied in the literature by changing the experimental variables, such as T, E_{appl}, f, and crystallographic orientation. We argue that people were essentially working on P_r (T, E_{appl}, f, crystallographic orientation) dependence of the fatigue properties. Knowing the analytical or empirical function of P_r (T, E_{appl}, f, crystallographic orientation) for a specific sample and inserting it into Eq. (19), we can readily derive the $T/E_{appl}/f/$orientation dependence of $P_r(N)$. That is the reason why we combined these dependences below into one section.

In Fig. 4, the $P_r(\equiv P_r(0))$ dependence of $P_r(N)$ according to Eq. (19) has been plotted, with P_r=10, 15, 18, and 20 μC/cm^2, respectively, where we take ε_i=40, D=0.9, F=0.1, and $A=10^{-9}$. It can be seen that the higher the P_r, the earlier fatigue will start and that low enough P_r results in fatigue-free behavior. This tendency has been generally observed in previous work.[30,37,38] Therefore, apart from lack of size effect, low P_r (normally less than 10 μC/cm^2) may also be one reason for the fatigue-free Pt/SBT/Pt structure.

Unfortunately, many researchers usually plot normalized $P_r(N)$ as function of N without showing the absolute $P_r(0)$ value, which is not recommended. We should also note that

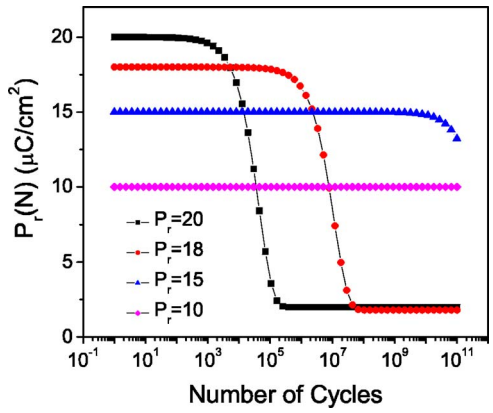

FIG. 4. (Color online) Plots of $P_r(N)$ as function of cycle number N, according to Eq. (19), where $P_r=10$, 15, 18, and 20, respectively. Here we take $\varepsilon_i=40$, $D=0.9$, $F=0.1$, and $A=10^{-9}$.

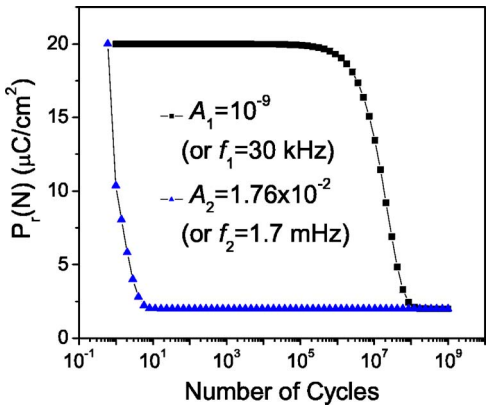

FIG. 5. (Color online) Plots of $P_r(N)$ as function of cycle number N, according to Eq. (19), where $A_1=10^{-9}$ for $f_1=30$ kHz and $A_2=1.76\times10^{-2}$ for $f_2=1.7$ mHz. Here we take $P_r=20$, $\varepsilon_i=45$, $D=0.9$, and $F=0.1$. Note that it shows a remarkably similar feature to Fig. 2 of the work of Colla *et al.* (Ref. 11).

the $P_r(N)$ in $P_r(N)\sim N$ plots in some papers may be different from the one discussed in our model, because they were evaluated after a certain number of electrical cycles from the hysteresis measurements using triangular and/or sine curves [or PUND (positive-up—negative-down) measurements used by Radiant Technologies], which may use different frequencies and/or voltages from those used in the fatigue tests.

1. Electrical field dependence

The applied field can be involved in fatigue by changing P_r, which is strongly field-dependent. Unfortunately, there is no simple analytic relationship between these two, although empirical equations can be built up by fitting $P_r\sim E_{appl}$ data. Normally, P_r increases significantly from zero when E_{appl} is approximately E_c-2E_c, and subsequently becomes saturated when E_{appl} approaches a few E_c.[25] Therefore, our model predicts fatigue-free behavior when E_{appl} is very small, due to either a lack of nucleation or a small P_r, a strongly field-dependent behavior when E_{appl} is close to $2E_c$, and a less field-dependent behavior when E_{appl} is so large that P_r is saturated. It should be noted that all the above arguments are based on "sufficient switching" conditions. If the switching is not sufficient, P_r will depend not only on E_{appl}, but also on frequency f (or pulse width). For experimental evidences of our argument, readers are referred to the works by Grossmann *et al.*,[39] Mihara *et al.*,[18] Chae *et al.*,[40] Amanuma *et al.*,[38] and Schorn *et al.*[41]

2. Cycling number, frequency, and embryonic time dependence

For most of the published fatigue studies, f is about 1 kHz–1 MHz, in which cases t_{pg} may be in nanoseconds and almost constant (we assume sufficient switching conditions here, which is equivalent to saying that P_r is independent of f). Therefore, in these cases, fatigue is sensitive only to N, not f, which can been seen from the literature.[39,40] Under "insufficient switching" conditions, the frequency (pulse width) dependence of fatigue can creep in by modifying P_r, as we discussed above. In those cases, it is generally observed that lower frequencies resulting in larger P_r induce more serious fatigue.[37]

Let us consider the effect of t_{pg} (or precisely the t_{em} part), a parameter which has never been considered in the literature and could provide strong evidence for our model. An interesting study was published by Colla *et al.*, where the film was fatigued either at a standard frequency (30 kHz) or an extremely low frequency (1.7 mHz).[11] In this work, serious fatigue was achieved with less than ten slow cycles (Fig. 2 in Ref. 11). Additionally, the authors conducted another "artificial" fatigue study (Fig. 3 in Ref. 11) by which the important role of $E_{appl}\sim E_c$ (i.e., a plateau E_{appl} applied at the coercive level E_c and slightly less than E_c) was identified, at least for the extremely low frequency ($\sim$1.7 mHz). Both of the experiments can be readily interpreted by our model without including separate mechanisms, as employed by these authors. For either of these two sets of experiments, the setup inducing serious fatigue corresponds to a dramatically increased t_{em} due to the elongated time at $E_{appl}\leqslant E_c$.

Let us suppose that A, the decomposition probability per unit power density per cycle, is proportional to t_{em}, which is proportional to $1/f$. Since $f_1=30$ kHz and $f_2=1.7$ mHz in their experiments, considering $A_1f_1=A_2f_2$, we have $A_2/A_1=f_1/f_2=1.76\times10^7$. Taking $A_1=10^{-9}$, we have $A_2=1.76\times10^{-2}$. The A dependence of $P_r(N)$ according to Eq. (19) has been plotted in Fig. 5, where $P_r=20$, $\varepsilon_i=45$, $D=0.9$, and $F=0.1$. Note that Fig. 5 shows a marked similarity to Fig. 2 in the work of Colla *et al.*[11] In particular, 7 orders of magnitude decrease of the fatigue endurance is predicted for 1.7 mHz compared with 30 kHz by our model, which was exactly what Colla *et al.* observed in this work. Note that the frequency-dependent fatigue data of Colla *et al.* have also been successfully modeled by Dawber and Scott.[4]

3. Temperature dependence

It is clear from our above argument that there are at least three temperatures involved in a fatigue experiment: the ambient temperature at which the experiment is conducted (e.g., 20 °C), the average sample temperature as measured by Lente and Eiras ($\sim$100 °C), and the local temperature which eventually induces the local decomposition ($\sim$700 °C,

which is yet unknown). Therefore, great care should be taken when data on T dependence are interpreted. An activation energy as low as 0.051 eV has been reported by Mihara *et al.* for PZT, which suggests that the fatigue mechanism is not influenced directly by the total amount of carriers or the thermal activation process over the trapping levels of defects.[18]

From our model's point of view, this complexity can also be understood. Let us take a PZT thin film fatigued at room temperature and higher temperatures as an example. The film fatigued at higher temperatures (e.g., 150 °C) has a lower P_r, which increases fatigue resistivity, but higher T may favor the local phase degradation by modifying the decomposition probability $A(T)$ in Eq. (19) and therefore, decrease fatigue resistivity. So the resultant $P_r(N) \sim N$ profile may be very independent of temperature, as observed by Mihara *et al.* Alternatively, it may be determined by the dominant factor.

Suppose, however, that $P_r(T)$ does play a dominant role. In this case, temperature can be involved in fatigue by changing P_r via $P_r \sim (T_c - T)^{\beta}$ near the transition point. For second-order phase transitions in mean-field theory, $\beta = 1/2$.

The complexity of the T dependence explained above even makes any qualitative interpretation extremely difficult, if not impossible. Indeed both improvement[18,42,43] and deterioration[44,45] of fatigue endurance at higher temperatures have been reported in the literature.

4. Fatigue anisotropy

From Eq. (4), E_{bc} is proportional to P_r. The latter is strongly orientation dependent. According to Fig. 4, the orientation with larger P_r should show faster fatigue rate than those with lower P_r. This has been confirmed by Takemura *et al.*[30] [Fig. 12(a) in their paper on single-crystal $Pb(Zn_{1/3}Nb_{2/3})O_3$-$PbTiO_3$]

D. Formation of oxygen-deficient layer and fatigue

Our model shows that the decomposed interface layer may be "pyrochlorelike," and is oxygen- (and probably lead-) deficient at the Pt/PPZT interface, which has been quantitatively confirmed by work from Scott *et al.*[46] and Mihara *et al.*[25] In both experiments, a significant decrease of oxygen concentration at the Pt/PZT interface has been observed in the seriously fatigued sample compared with the virgin one. Note that the depth profile of Pb ions was not monitored in these measurements.

The data of Pan *et al.*,[47] which imply oxygen leaving a PZT sample during fatigue, are consistent with the observations of Scott *et al.* and Mihara *et al.* within our model.

E. Optical, thermal fatigue, and rejuvenation by a high field

We believe that although standard electrical fatigue, i.e., suppression of remanent polarization by applying bipolar electrical cycles, seems to be induced directly by local phase decomposition from the present work, fatigue, in a general sense, can also be induced by specially designed methods such as optical, thermal, and even reducing processes, as nicely shown in a series of papers by Warren and co-workers.[6,48–55] Whether or not a local degraded phase is also formed at the nucleation sites in these processes is currently unknown and warrants further exploration, but an interesting point about this work is that both optical fatigue and thermal fatigue are maximized by illuminating the material with band-gap light in case of optical fatigue (or heating it to ~100 °C in case of thermal fatigue) in combination with biasing the ferroelectric near the switching threshold (below the coercive field). The importance of the switching threshold field on fatigue has been extensively discussed in the previous section, particularly regarding the extremely low frequency (subhertz) fatigue data of Colla *et al.* Our model shows that the probability of failure of the nucleation site at the switching threshold field increases dramatically. Therefore, the data by Warren *et al.* may be compatible with our model, and a generalized version of our model might also be able to interpret optical and/or thermal fatigue quantitatively. In these processes, coefficient A in Eq. (19) strongly depends on time (or frequency) in the work of Colla *et al.*, power and illuminating time of band-gap light (for optical fatigue), and temperature and heating time (for thermal fatigue) in the work of Warren and co-workers. It will eventually determine the profile of the $P_r(N) \sim N$ plot. From the physical point of view, the photoelectrons produced by illuminating UV light (or thermally excited electrons produced by heating) will either help "destroy" the existing nuclei when a threshold positive voltage, i.e., +2 V in the work of Warren and co-workers, is applied, or help "create" new nuclei when a saturating negative bias voltage, i.e., −15 V in the work of Warren and co-workers, is applied. Therefore, this is indeed compatible with our model. However, unlike the data of Colla *et al.*, these optical and/or thermal fatigue experiments were conducted in a rather qualitative way. Therefore we will not develop a quantitative description for them until further experiments are carried out.

Although its effect in rejuvenating the remanent polarization is maximized in combination with UV light, a pure high dc and/or ac field itself may also be able to create some new nucleation sites, without affecting the fatigue-induced degraded sites. Depending on the efficiency of this field in doing so, different degrees of the refreshment of the fatigued sample have been reported, such as no or little recovery as observed in the literature and this work (not shown here), partially recovery,[56] and full recovery.[57]

However, it should be noted that even though the rejuvenation is almost complete in terms of the remnant polarization, it can never refresh the fatigued film to its initial state. An increase in the width of the hysteresis loop (i.e., $2V_c$, coercive voltage) was usually reported.[6] Furthermore, the rejuvenated fatigued film by either UV and/or saturating bias combination[6] or pure high electric pulse[57] always refatigues more rapidly, confirming that the rejuvenation is incomplete. This indicates that some irreversible damage has occurred that could not be removed by the restore methods, which is also in accordance with our model, because the decomposed phase cannot be simply recovered by applying an electrical restore field (or combined with UV light).

F. Unipolar and bipolar fatigue

It is well known that unipolar pulses lead to much less fatigue on the same sample compared with bipolar ones.[58]

That is very obvious from our model. Without the processes of nucleation and subsequent needle domain growth (Fig. 1), there is no large depolarization field experienced by the sample and so no decomposition takes place in unipolar cycling; therefore, it results in little or no fatigue.

This is also consistent with the well-accepted view that applying an electric field which is larger than the coercive field is a necessary condition for inducing bipolar fatigue. Additionally, from our model, it is also understandable why applying a small field (less than E_c) often results in a "fatigue-free" Pt/PZT/Pt structure as shown in some careless publication.

G. Microcracks and fatigue

Microcracks can be easily deduced by the strain after local phase decomposition during fatigue. Therefore microcracks (or cracks in fatigued ceramics) are the result instead of the cause of fatigue, as already suspected by many researchers. The formation of microcracks (or cracks) is another strong evidence for our model, since most of the other fatigue models fail to explain this phenomenon.

H. Porosity, grain size, and fatigue

This model indicates that more porous ceramics or samples with larger grain size should show faster fatigue rates because of the larger mean free path and higher kinetic energy of the injected energetic electrons flying through the pores and/or the voids within the nucleation site at the interface, which has been confirmed by Jiang *et al.*[59,60]

IV. CONCLUSIONS

A different fatigue model has been established by taking into consideration the extremely high unscreened field that the head-to-head bound charges produced during switching at the near-electrode regions. This field produces an intensive injected current, which eventually cause local phase decomposition at the nucleation sites, and consequently, fatigue. The relationship $P_r(N)/P_r(0) \sim \exp(-N/\lambda)$ derived from our model interprets the *statistical* origin of the *universality* of the logarithmic feature in $P_r(N) \sim N$ plots in the literature for various ferroelectric materials. Furthermore, the size effect/fatigue coupling, the fatigue-free phenomenon for low-P_r samples, as well as the "artificial" fatigue data of Colla *et al.* performed at an extremely low frequency are all compatible with our model. The consistency of this model with the experimental data previously published has been discussed, and a systematic picture of fatigue is built up.

ACKNOWLEDGMENTS

X.J.L. would like to thank Cambridge Overseas Trust for support during this work. We are indebted to E. A. Kafadaryan for kindly providing the PZT films.

*Author to whom correspondence should be addressed. Email address: XL217@cam.ac.uk

[1] J. F. Scott, *Ferroelectric Memories* (Springer, New York, 2000).
[2] C. A. P. de Araujo, J. D. Cuchiaro, L. D. McMillan, M. C. Scott, and J. F. Scott, Nature (London) **374**, 627 (1995).
[3] J. F. Scott, Integr. Ferroelectr. **38**, 769 (2001).
[4] M. Dawber and J. F. Scott, Appl. Phys. Lett. **76**, 1060 (2000); **76**, 3655 (2000).
[5] J. F. Scott and M. Dawber, Appl. Phys. Lett. **76**, 3801 (2000).
[6] W. L. Warren, D. Dimos, B. A. Tuttle, G. E. Pike, R. W. Schwartz, P. J. Clews, and D. C. McIntyre, J. Appl. Phys. **77**, 6695 (1995).
[7] P. K. Larsen, G. J. M. Dormans, D. J. Taylor, and P. J. Vanveldhoven, J. Appl. Phys. **76**, 2405 (1994).
[8] J. J. Lee, C. L. Thio, and S. B. Desu, J. Appl. Phys. **78**, 5073 (1995).
[9] A. M. Bratkovsky and A. P. Levanyuk, Phys. Rev. B **63**, 132103 (2001).
[10] A. M. Bratkovsky and A. P. Levanyuk, Phys. Rev. Lett. **84**, 3177 (2000).
[11] E. L. Colla, D. V. Taylor, A. K. Tagantsev, and N. Setter, Appl. Phys. Lett. **72**, 2478 (1998).
[12] A. K. Tagantsev, I. Stolichnov, E. L. Colla, and N. Setter, J. Appl. Phys. **90**, 1387 (2001).
[13] Q. Y. Jiang, W. W. Cao, and L. E. Cross, J. Am. Ceram. Soc. **77**, 211 (1994).
[14] X. J. Lou, M. Zhang, S. A. T. Redfern, and J. F. Scott, Phys. Rev. Lett. **97**, 177601 (2006).
[15] V. V. Lemanov and V. K. Yarmarkin, Ferroelectrics **201**, 55 (1997).
[16] K. Szot, W. Speier, G. Bihlmayer, and R. Waser, Nat. Mater. **5**, 312 (2006).
[17] B. M. Melnick, J. F. Scott, C. A. P. Dearaujo, and L. D. McMillan, Ferroelectrics **135**, 163 (1992).
[18] T. Mihara, H. Watanabe, and C. A. P. de Araujo, Jpn. J. Appl. Phys., Part 1 **33**, 3996 (1994).
[19] J. Li, B. Nagaraj, H. Liang, W. Cao, C. H. Lee, and R. Ramesh, Appl. Phys. Lett. **84**, 1174 (2004).
[20] R. J. Harrison, S. A. T. Redfern, and E. K. H. Salje, Phys. Rev. B **69**, 144101 (2004).
[21] C. B. Parker, J. P. Maria, and A. I. Kingon, Appl. Phys. Lett. **81**, 340 (2002).
[22] J. F. Scott, D. Galt, J. C. Price, J. A. Beall, R. H. Ono, C. A. P. Dearaujo, and L. D. McMillan, Integr. Ferroelectr. **6**, 189 (1995).
[23] J. F. Scott, B. M. Melnick, L. D. McMillan, and C. P. de Araujo, Integr. Ferroelectr. **3**, 225 (1993).
[24] S. M. Sze, *Physics of Semiconductor Devices* (Wiley-Interscience, New York, 1981).
[25] T. Mihara, H. Watanabe, and C. A. P. de Araujo, Jpn. J. Appl. Phys., Part 1 **33**, 5281 (1994).
[26] M. H. Lente and J. A. Eiras, J. Phys.: Condens. Matter **12**, 5939 (2000).
[27] S. Y. Chen and I. W. Chen, J. Am. Ceram. Soc. **77**, 2337 (1994).
[28] R. N. Castellano and L. G. Feinstein, J. Appl. Phys. **50**, 4406

(1979).
[29] H. Tabata, T. Kawai, S. Kawai, O. Murata, J. Fujioka, and S. Minakata, Appl. Phys. Lett. **59**, 2354 (1991).
[30] K. Takemura, M. Ozgul, V. Bornand, S. Trolier-McKinstry, and C. A. Randall, J. Appl. Phys. **88**, 7272 (2000).
[31] B. T. Lee and C. S. Hwang, Appl. Phys. Lett. **77**, 124 (2000).
[32] H. M. Duiker, P. D. Beale, J. F. Scott, C. A. P. de Araujo, B. M. Melnick, J. D. Cuchiaro, and L. D. McMillan, J. Appl. Phys. **68**, 5783 (1990).
[33] H. Z. Jin and J. Zhu, J. Appl. Phys. **92**, 4594 (2002).
[34] E. L. Colla, S. B. Hong, D. V. Taylor, A. K. Tagantsev, N. Setter, and K. No, Appl. Phys. Lett. **72**, 2763 (1998).
[35] A. Gruverman, O. Auciello, and H. Tokumoto, Appl. Phys. Lett. **69**, 3191 (1996).
[36] C. Verdier, F. D. Morrison, D. C. Lupascu, and J. F. Scott, J. Appl. Phys. **97**, 024107 (2005).
[37] A. Morimoto, Y. Yamanaka, and T. Shimizu, Jpn. J. Appl. Phys., Part 1 **34**, 4108 (1995).
[38] K. Amanuma, T. Hase, and Y. Miyasaka, Jpn. J. Appl. Phys., Part 1 **33**, 5211 (1994).
[39] M. Grossmann, D. Bolten, O. Lohse, U. Boettger, R. Waser, and S. Tiedke, Appl. Phys. Lett. **77**, 1894 (2000).
[40] B. G. Chae, C. H. Park, Y. S. Yang, and M. S. Jang, Appl. Phys. Lett. **75**, 2135 (1999).
[41] P. J. Schorn, D. Brauhaus, U. Bottger, R. Waser, G. Beitel, N. Nagel, and R. Bruchhaus, J. Appl. Phys. **99**, 114104 (2006).
[42] M. Ozgul, K. Takemura, S. Trolier-McKinstry, and C. A. Randall, J. Appl. Phys. **89**, 5100 (2001).
[43] D. Wang, Y. Fotinich, and G. P. Carman, J. Appl. Phys. **83**, 5342 (1998).
[44] E. Paton, M. Brazier, S. Mansour, and A. Bement, Integr. Ferroelectr. **18**, 29 (1997).
[45] G. L. Yuan, J. M. Liu, Y. P. Wang, D. Wu, S. T. Zhang, Q. Y. Shao, and Z. G. Liu, Appl. Phys. Lett. **84**, 3352 (2004).
[46] J. F. Scott, C. A. Araujo, B. M. Melnick, L. D. McMillan, and R. Zuleeg, J. Appl. Phys. **70**, 382 (1991).
[47] M. J. Pan, S. E. Park, C. W. Park, K. A. Markowski, S. Yoshikawa, and C. A. Randall, J. Am. Ceram. Soc. **79**, 2971 (1996).
[48] W. L. Warren, B. A. Tuttle, and D. Dimos, Appl. Phys. Lett. **67**, 1426 (1995).
[49] H. N. AlShareef, D. Dimos, T. J. Boyle, W. L. Warren, and B. A. Tuttle, Appl. Phys. Lett. **68**, 690 (1996).
[50] H. N. AlShareef, D. Dimos, W. L. Warren, and B. A. Tuttle, Integr. Ferroelectr. **15**, 53 (1997).
[51] D. Dimos, H. N. AlShareef, W. L. Warren, and B. A. Tuttle, J. Appl. Phys. **80**, 1682 (1996).
[52] D. Dimos, W. L. Warren, M. B. Sinclair, B. A. Tuttle, and R. W. Schwartz, J. Appl. Phys. **76**, 4305 (1994).
[53] W. L. Warren, D. Dimos, H. N. AlShareef, M. V. Raymond, B. A. Tuttle, and G. E. Pike, J. Am. Ceram. Soc. **79**, 1714 (1996).
[54] W. L. Warren, D. Dimos, B. A. Tuttle, R. D. Nasby, and G. E. Pike, Appl. Phys. Lett. **65**, 1018 (1994).
[55] W. L. Warren, D. Dimos, B. A. Tuttle, G. E. Pike, and H. N. AlShareef, Integr. Ferroelectr. **16**, 77 (1997).
[56] M. Ozgul, S. Trolier-McKinstry, and C. A. Randall, J. Appl. Phys. **95**, 4296 (2004).
[57] J. F. Scott and B. Pouligny, J. Appl. Phys. **64**, 1547 (1988).
[58] C. Verdier, D. C. Lupascu, and J. Rodel, J. Eur. Ceram. Soc. **23**, 1409 (2003).
[59] Q. Y. Jiang and L. E. Cross, J. Mater. Sci. **28**, 4536 (1993).
[60] Q. Y. Jiang, E. C. Subbarao, and L. E. Cross, Acta Metall. Mater. **42**, 3687 (1994).